



Staphylococcus epidermidis biofilm assembly and self-dispersion: bacteria and matrix dynamics

Suzanne Jonblat^{1,2,3,4} · Falah As-sadi^{1,5} · Kazem Zibara⁶ · Marwan El Sabban⁷ · Vera Dermesrobian^{7,8} · André El Khoury⁴ · Mireille Kallassy³ · Ali Chokr^{1,2}

Received: 8 August 2023 / Revised: 17 September 2023 / Accepted: 25 September 2023
© The Author(s), under exclusive licence to Springer Nature Switzerland AG 2023

Abstract

Staphylococcus epidermidis, despite being a commensal of human skin and mucosa, is a major nosocomial pathogen implicated in device-associated infections. The dissemination of infection to other body sites is related to biofilm dispersal. This study focused on the dispersion stage of *S. epidermidis* CIP 444 biofilm, with the assessment of biofilm matrix composition in a time-dependent experiment (7 days extended) with 3 independent repetitions, using confocal laser scanning microscopy (CLSM) in association with ZEN 3.4 blue edition, COMSTAT, and ImageJ software. SYTO-9, propidium iodide (PI), DID'OIL, FITC, and calcofluor white M2R (CFW) were used to stain biofilm components. The results indicated that the biomass of dead cells increased from $15.18 \pm 1.81 \mu\text{m}^3/\mu\text{m}^2$ (day 3) to $23.15 \pm 6.075 \mu\text{m}^3/\mu\text{m}^2$ (day 4), along with a decrease in alive cells' biomass from $22.75 \pm 2.968 \mu\text{m}^3/\mu\text{m}^2$ (day 3) to $18.95 \pm 5.713 \mu\text{m}^3/\mu\text{m}^2$ (day 4). When the intensities were measured after marking the biofilm components, in a 24-h-old biofilm, polysaccharide made up the majority of the investigated components (52%), followed by protein (18.9%). Lipids make up just 11.6% of the mature biofilm. Protein makes up the largest portion (48%) of a 4-day-old biofilm, followed by polysaccharides (37.8%) and lipids (7.27%). According to our findings, *S. epidermidis* CIP 444 dispersion occurred on day 4 of incubation, and new establishment of the biofilm occurred on day 7. Remarkable changes in biofilm composition will pave the way for a new approach to understanding bacterial strategies inside biofilms and finding solutions to their impacts in the medical field.

Keywords Biofilm · Dispersion · Clsm · *Staphylococcus epidermidis*

✉ Ali Chokr
alichokr@hotmail.com

¹ Research Laboratory of Microbiology (RLM), Department of Life and Earth Sciences, Faculty of Sciences I, Lebanese University, Hadat Campus, Beirut, Lebanon

² Platform of Research and Analysis in Environmental Sciences (PRASE), Doctoral School of Sciences and Technologies, Lebanese University, Hadat Campus, Beirut, Lebanon

³ Functional Genomics and Proteomic Laboratory, Faculté Des Sciences, Université Saint-Joseph de Beyrouth, Campus Des Sciences Et Technologies, Mar Roukos, Matn, Lebanon

⁴ Centre d'Analyses Et de Recherche (CAR), Unité de Recherche Technologies Et Valorisation Agro-Alimentaire (UR-TVA), Faculté Des Sciences, Université Saint-Joseph

de Beyrouth, Campus Des Sciences Et Technologies, Mar Roukos, Matn, Lebanon

⁵ Department of Plant Production, Faculty of Agriculture and Veterinary Medicine, Lebanese University, Beirut 999095, Lebanon

⁶ ER045, Laboratory of Stem Cells, DSST, Biology Department, Faculty of Sciences-I, Lebanese University, Beirut, Lebanon

⁷ Department of Anatomy, Cell Biology and Physiological Sciences, Faculty of Medicine, American University of Beirut, Bliss Street, Beirut 1107, Lebanon

⁸ Present Address: Department of Microbiology, Immunology and Transplantation, Laboratory of Adaptive Immunity, KU Leuven, Louvain, Belgium

Introduction

All medical devices or tissue engineering constructs are susceptible to microbial colonization and infection (Byers and Ratner 2004; Castelli et al. 2006).

Biofilm-embedded pathogens had a 1000-fold increase in their antibiotic tolerance in contrast to their genetically equivalent planktonic bacteria (Rogers et al. 2010). The fourth main cause of death in the USA that increases the medical cost by more than \$5 billion per year is hospital-acquired infections (nosocomial), with 2 million cases annually, especially catheter- and implant-related infections, which were a major contributor (60–70%) to the increase in nosocomial infections (Safdar & Maki 2002; Wenzel 2007; Ecker & Carroll 2005). Although being a part of the normal human flora, mainly the skin and mucosal flora, *Staphylococcus epidermidis*, a coagulase-negative *staphylococcus* (CoNS), has been considered a major nosocomial pathogen, capable of biofilm formation, infecting surgical wounds, and causing infections associated with indwelling medical devices; hence, it is responsible for 30 to 43% of joint prosthesis infections and for 50–70% of catheter-related infections (Rupp & Archer 1994). Being a permanent colonizer of human skin enables *S. epidermidis* to frequently contaminate medical devices and implants during insertion at a high rate (Suryabrata 2008). Studies have linked virulence to the biofilm process, whereas the production of polysaccharide intracellular adhesin (PIA) promotes bacterial protection against antibiotics. The essential pathogenesis of *S. epidermidis* infection is due to the formation of biofilm, which is a complex interaction of unicellular organisms encased in an extracellular matrix of polysaccharides, proteins, and nucleic acids. The process of biofilm formation is composed of at least three phases, beginning with adherence and primary attachment, where bacteria adhere to a surface, then, in the second phase, accumulate themselves by forming a 3D multicellular architecture with multiple layers without attaching themselves directly to the surface (Mack et al. 2009; Otto 2009; Rohde et al. 2010). After this phase, the cells are detached autonomously from the assembly, where *S. epidermidis* is capable of colonizing other body sites. However, this process is a combination of a wide range of molecules acting in each phase, including binding to the surface, cell–cell aggregation, and disrupting matrix components (Otto 2009). Studies concerning the chemical composition of biofilms are expanding due to their role in disease detection and diagnosis, for example, using poly-*N*-acetylglucosamine and its de-*N*-acetylated epitope as antigens to elicit an immune response during infection. Although this method helped in detecting infection, it was not valuable in all cases (Sadovskaya et al.

2007). As for its composition, up to 97% of biofilm is water, and the remaining is extracellular polymeric substances (EPS) produced by the microbial cells (Zhang et al. 1998).

The importance of studying the biochemical composition of biofilm lies in understanding and monitoring proteins and enzymes that are induced in response to various stimuli, such as resisting a specific antibiotic. For example, in the case of *Pseudomonas aeruginosa*, resistance to different antibiotics in cystic fibrosis was due to the overexpression of cephalosporinase Amp C enzymes, which are the main contributors to biofilm formation in *P. aeruginosa* (Rojas and Valle 2009). Sadovskaya et al. characterized 66 strains of CoNS associated with medical implant infections, including several potentially virulent strains of *S. epidermidis*. Three out of 11 investigated clinical staphylococcal strains (*S. epidermidis* 5, *S. epidermidis* CIP 444, and *S. aureus* 343) that developed biofilms in vitro produced significant levels of PNAG (Sadovskaya et al. 2006). The polysaccharide with the poly-(1,6)-*N*-acetyl- β -D-glucosamine backbone was produced by all PNAG-producing strains, with varying degrees of *N*-deacetylation and *O*-succinylation. The chemical make-up of the biofilms' extracellular matrix was positively linked with how susceptible they were to various enzymatic treatments. Therefore, another strategy in dispersing the biofilm is to disintegrate the polysaccharides; thus, studying the biochemical variations in the biofilm is a key role in investigating new approaches towards its elimination. Gonzalez-Machado et al. (2018) conducted a quantitative study on biofilm formation that analyzed and differentiated between the cells, proteins, lipids, -polysaccharides, and -polysaccharide content in the *Salmonella agona* biofilm at different stages of development based on confocal laser scanning microscopy (CLSM) and image analysis techniques.

For the microscopic visualization of biofilms, confocal laser scanning microscopy (CLSM) has become the imaging technique with the broadest use (Azeredo et al. 2017; Ben-Sahil et al. 2020). A flexible and effective method, CLSM enables 3D reconstruction of the entire sample as well as in situ, real-time, and nondestructive study of live biofilms. For this, CLSM excites fluorescence signals from several sample planes, leading to the capture of many images from the depth of the biofilm. Insights into the formation, growth, morphology, structure, and architecture of biofilms under various circumstances have been obtained through CLSM's ability to conduct qualitative observations of clinical, environmental, and laboratory biofilms. Additionally, with some adjustments, CLSM has been used to evaluate the vitality and species diversity of biofilms (Mountcastle et al. 2021). The use of CLSM for biofilm investigations has lately progressed beyond simple descriptive observations to a more in-depth analysis of biofilms using high-resolution image

stacks (Dhekane et al. 2022). For this, image analysis methods and CLSM are coupled because they may together offer quantitative insights on biofilm properties under various circumstances. These image analysis applications include tools for processing images that may be used widely, such as ImageJ and IMARIS, as well as tools specifically designed for studying biofilms, including COMSTAT and BiofilmQ (Jeckel and Drescher 2021).

In this study, the *S. epidermidis* biofilm matrix was analyzed by 3D imaging using CLSM at the dispersion stage of the biofilm. This would appear to be the first time that a quantitative *S. epidermidis* biofilm's analysis of live cells, dead cells, proteins, lipids, and -polysaccharide content has been studied. This work is a novel research project in *S. epidermidis* biofilm, focusing on the detachment phase in addition to studying the spatial distribution of the components inside the biofilm at different stages of its life cycle. Thus, determining the changes that encounter the biochemical structure during its cycle that is a fundamental strategy for understanding, controlling, and modeling biofilms formed by pathogenic bacteria.

Materials and methods

Bacterial Strain

The Gram-positive bacterium *S. epidermidis* CIP 444 was used in this study. It is a clinical strain that was isolated from a patient with an infected implanted device hospitalized in the Mignot Hospital of Versailles, France. This strain was

identified and characterized for many features in the previous studies and deposited to be enclosed within the microorganisms of the collection of the Pasteur Institute, Paris, in 2007.

Biofilm preparation

S. epidermidis CIP 444 was cultured in tryptic soy broth (TSB) from Himedia (Mumbai, India) for 18 h at 37 °C. A concentration of 1×10^6 CFU/mL from the preculture was added to a total volume of 300 μ L of TSB supplemented with 0.25% wt/vol glucose in a glass coverslip-bottom dish (50-mm dish, no. 1.5, 14-mm coverslip diameter) (MatTek Co., Falcon, USA) and incubated at 37 °C for different periods of time from 1 to 7 days. In order to prevent evaporation during incubation, an optimization study was conducted to indicate the best conditions for biofilm formation, including TSB volume and the culturing support (glass or polystyrene) (data not shown). The experiment was done in triplicate and with three independent repetitions.

Staining procedure and confocal imaging

Five fluorescent dyes were used for the staining procedure (Table 1). SYTO 9 and propidium iodide (PI) from the LIVE/DEAD Bac Light™ bacterial viability kit, DiIC₁₈(5) oil, 1,1'-dioctadecyl-3,3',3'-tetramethylindodicarbocyanine perchlorate (DID'OIL) were purchased from Invitrogen™ (Carlsbad, CA, United States), while fluorescein isothiocyanate isomer I (FITC) and calcofluor white M2R (CFW) were purchased from Sigma-Aldrich® (St. Louis, Missouri, United States).

Table 1 Stains and microscopic parameters used in studying the cellular and extracellular components of the biofilms formed by *S. epidermidis* CIP 444

Dyes	SYTO9 ^a	PI ^b	CFW ^c	DID'OIL ^d	FITC ^e
Laser wavelength	488 nm: 2.00%	561 nm: 9.00%	405 nm: 5.00%	514 nm: 30.00%	488 nm: 4.00%
Excitation wavelength	488 nm	561 nm	405 nm	514 nm	488 nm
Emission wavelength	559 nm	642 nm	450 nm	596 nm	464 nm
Detection wavelength	505–613 nm	566–718 nm	410–490 nm	519–672 nm	493–634 nm
Image device	LSM710/Axio observer	LSM710/Axio observer	LSM710/Axio observer	LSM710/Axio observer	LSM710/Axio observer
Detector	PMT	PMT	PMT	PMT	PMT
Detector gain	480 V	850 V	800 V	900 V	650 V
Target	Live cells	Dead cells	B-polysaccharide	Lipids	Proteins

^a**Syto 9** is a nucleic acid stain with green fluorescent

^b**Propidium iodide** is a nucleic acid stain impermeable to cells with red fluorescence

^c**Calcofluor white** is a fluorescent blue dye it binds to 1-3beta and 1-4 beta extracellular polysaccharide impermeable to intact cells

^d**DiIC₁₈(5) oil (1,1'-dioctadecyl-3,3',3'-tetramethylindodicarbocyanine perchlorate)** lipophilic carbocyanine membrane dye that labels cell membranes by inserting its two long (C18 carbon) hydrocarbon chains into the lipid bilayers; once applied to cells, it diffuses laterally within the plasma membrane and emits red–orange color

^e**Fluorescein isothiocyanate isomer** is a yellow-orange in color; upon excitation, it emits a yellow-green color; it is widely used to attach a fluorescent label to protein via the amine group

The stains were prepared as follows: SYTO 9 (stock 3.34 mM in DMSO) plus PI (stock 20 mM in DMSO) at 1.0 $\mu\text{L}/\text{mL}$ each; CFW at 189 $\mu\text{L}/\text{mL}$; DID'OIL (stock of 25 mg in 2.5 mL of absolute ethanol) at 79.4 $\mu\text{g}/\text{mL}$; and FITC (stock 2 mg in 100 μL of absolute ethanol) at 46.6 $\mu\text{g}/\text{mL}$. To avoid overlapping spectra, each dye was studied solely (Fig. 1). Additionally, the medium containing the planktonic sample was discarded, and the biofilm sample was washed with sterile distilled water, stained by the Bac Light live/dead bacterial viability kit according to manufacturer protocol, and incubated in the dark for 20 min for a group of samples. The other lot was stained with the latter, incubated for 20 min in the dark, followed by the addition of 1 drop of calcofluor white M2R for 1 min. The combination was done only for CFW, SYTO9, and PI to prevent signal crosstalk. For lipid and protein staining, 250 μL of the prepared stock solution of DID'OIL and FITC dyes was added to the biofilm sample separately and incubated for 30 min in the dark. The samples were washed after staining with sterile distilled water to remove any dye excess, then fixed with 4% (wt/vol) paraformaldehyde for another 20 min. To prevent the interference of PBS (from the paraformaldehyde) with the fluorescence of the dyes, the samples were gently washed again with distilled water three times.

Confocal laser scanning microscopy (CLSM) image examination was performed using a Zeiss LSM 710 Axio Observer confocal laser scanning microscope. Channel mode visualization was done using the $63\times, 100\times$ (Apochromat/1.40, M27) objective with oil immersion. Z-stacks of horizontal plane images (512×512 pixels corresponding to $134.95\ \mu\text{m}\times 134.95\ \mu\text{m}$) with a z-step of $0.39\ \mu\text{m}$ were acquired for each well from five

different randomly chosen areas where the maximum thickness (μm) of biofilms was determined directly from the confocal stack image. Three independent experiments with three replicates were performed for each sample during the biofilm life cycle over a 7-day period. In order to visualize the whole biofilm architecture in the well of the dish and to detect how the dispersion of the cells is influencing the biofilm structure and how its components interact and cover the bacteria. Therefore, 10x (Fig. 1), 20x and 63x magnification images were collected.

The images were analyzed using ZEISS, ZEN 3.4 blue edition (Carl Zeiss, Jena, German) software, a 3D model of the biofilm under study was obtained (Fig. 2), and the fluorescent intensities of all studied dyes were measured, which reflect the amount of the used dye in the sample of observation field area $1.42\ \text{cm}^2$.

Individual components of biofilm are the biomass, which is defined as the volume of all voxels (values in a grid) containing cells divided by their area. The height (z), width (x), and length (y) of a voxel (= biovolume) are multiplied by the total number of voxels; a number that is independent of the size of the observed area is obtained in $\mu\text{m}^3/\mu\text{m}^2$, by dividing the biovolume by the area of the substratum.

In other words, the biomass is an expression of how much of the image stack is covered by bacteria. The surface-to-volume ratio is calculated by measuring the surface area, which is obtained by looking at all of the voxels in the stack and counting the surfaces facing the void, and the volume from the biomass. Biofilm roughness (R_a^*) which determines the variation in the biofilm's height and thus biofilm heterogeneity. R_a^* equals zero, the biofilm surface is considered uniform. R_a^* is calculated by the software using the formula:

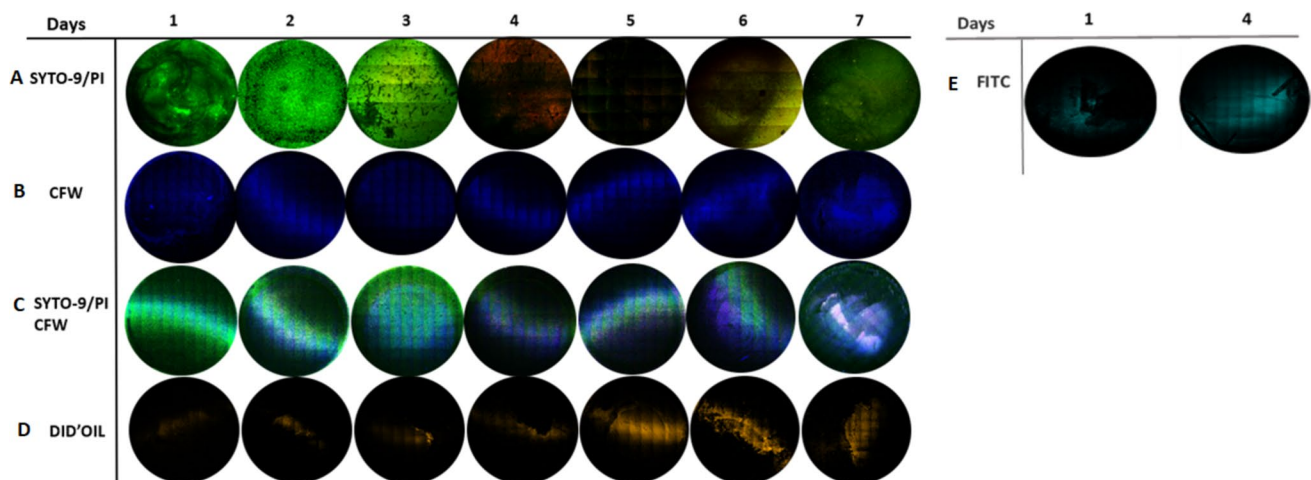


Fig. 1 CLSM images tile scan ($10\times$) of *S. epidermidis* 444 biofilm stained with different fluorescent dyes during 7 days of incubation. As it is shown in the observation field (wells), the whole biofilm with the changes encountering its components with respect to time. Scale bar = $1000\ \mu\text{m}$, area = $1.42\ \text{cm}^2$. **A** Corresponds to the LIVE/DEAD

staining of biofilm cells during the studied period, green for live and red for dead. **B** shows the polysaccharide staining and **C** the combination of three dyes showing the live, dead cells and polysaccharides. **D** lipid content in the biofilm over time and **E** protein profile for day 1 and 4

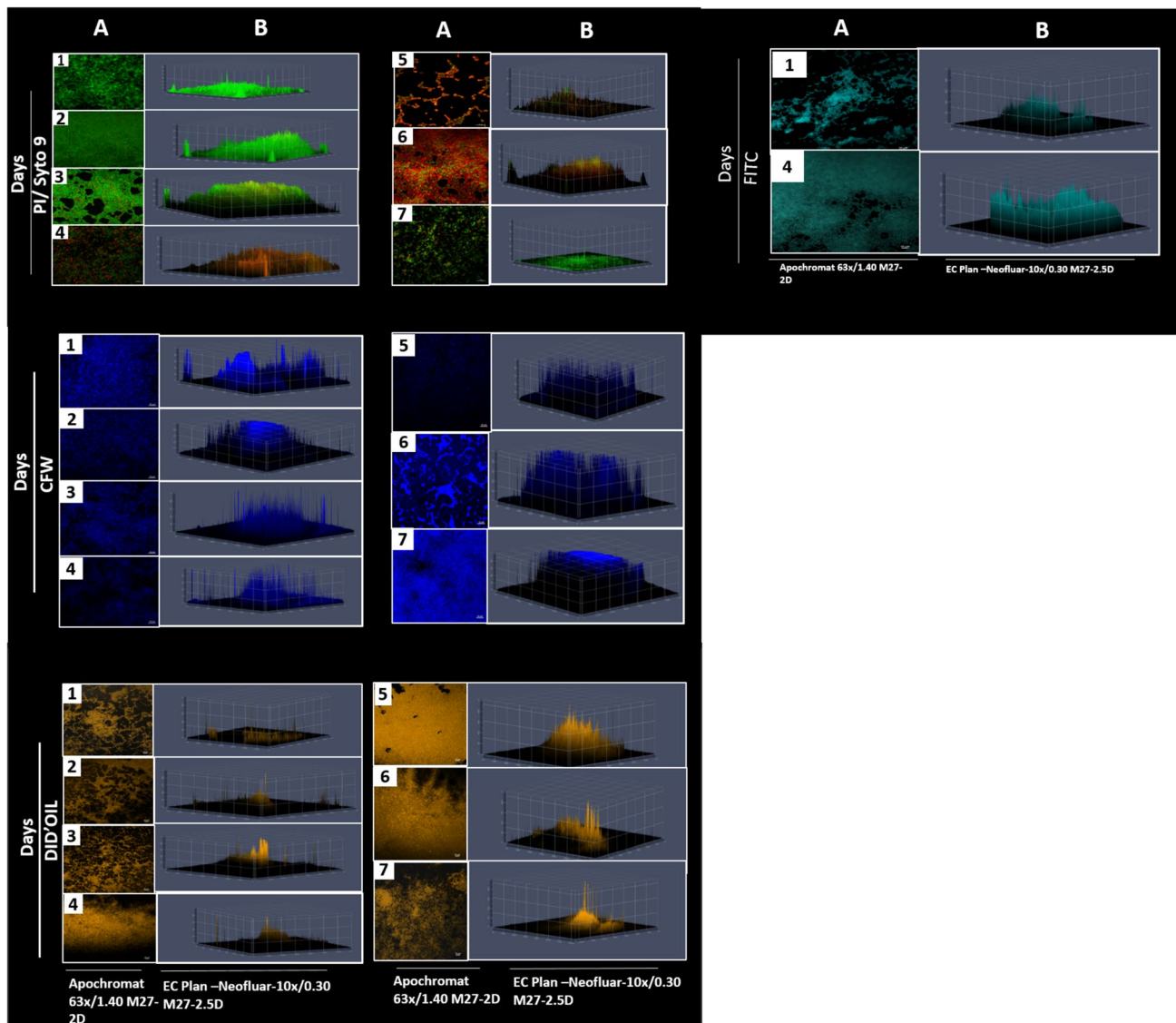


Fig. 2 Confocal laser scanning microscopy (CLSM) of *S. epidermidis* CIP (444) biofilm during 7 days after LIVE/DEAD Bac light bacterial viability kit staining in a confocal dish. Green fluorescence (Syto-9) indicates alive cells, red fluorescence (PI) stains dead cells. Changes in biofilm structure were remarkable (A), increase of red fluorescence from day 4 indicating high percentage of dead cells and disintegration of the biofilm, correlated with a decrease in biofilm

thickness as indicated in the 2.5D illustration (B). Biofilm regeneration and re-establishment from minimal resources sighted at day 7 with an increase in alive cells and the reformation of biofilm scaffold. Same procedure was repeated for the other dyes. Scale bar = 10 μ m Apochromat 63 \times /1.40 M27 (A), EC Plan-Neofluar 10 \times /0.30 M27 Tilescan 2.5D structure (B)

$$R_{\alpha}^{*} = \frac{1}{N} \sum_{i=1}^N \frac{|L_{fi} - \bar{L}_f|}{\bar{L}_f}$$

where N is the number of thickness measurements, L_{fi} is the thickness measured for the (i) time, and \bar{L}_f is the average thickness were quantified using COMSTAT 2.1 software (DTU, Denmark) (<http://www.comstat.dk/>) (Heydorn et al. 2000; Vorregaard 2008) through z-stacks of images represented by fluorescence emitted by SYTO-9 (from cells

with intact membranes) and PI (from bacteria with damaged membranes, eDNA). All images processed had the same size. An automatic threshold (Otsu's method) was applied in addition to the "connected volume filtering" (CVF) option, which is useful for preventing unrelated or detached biomass from being included in the analysis. The software calculates the biomass according to both channels (green and red). The spatial distribution of biofilm components was generated using ImageJ software (LOCI, University of Wisconsin, USA).

Statistical analysis

The quantitative structural parameters of the biofilm were submitted for statistical analysis using analysis of variance (ANOVA). Comparisons between means were carried out according to Duncan's multiple range test. The difference was considered significant at a P level of <0.05 . The experiment was carried out over three independent repetitions. Correlation (r) between intensities was conducted according to Pearson's test using the "R" program (R Foundation for Statistical Computing, Vienna, Austria) (<http://www.R-project.org>) in order to detect if the components are proportional according to the studied period or are independent from each other.

Results and discussion

Biofilm was stained with five different fluorescent dyes. 2D/2.5D images were obtained and analyzed via the ZEN Blue 3.4 Light version software (Figs. 1 and 2). Bac Light live/dead bacterial viability kit staining showed the fluctuation of dead vs. alive cells during the biofilm cycle by measuring the intensities of both fluorescent dyes and calculating the percentages of the two colors with respect to each other.

When comparing SYTO-9 to PI intensity in arbitrary units (a. u.), SYTO-9 (green fluorescence) was dominant in the first 3 days (SYTO-9 4.22 ± 1.565 a. u., PI 1.35 ± 0.7545 a. u. on day 3), indicating a healthy, alive, and mature biofilm. The green fluorescence decreased at day 4 (0.58 ± 0.1965 a. u.), and a progressive increase in dead cells and eDNA (PI, red fluorescence) was detected (4.23 ± 0.25 a. u.) (Fig. 3). Consequently, PI intensity was higher than SYTO-9 from day 4 to day 6. Hence, dead cells outnumber alive cells. If we want to relate this finding to the biofilm life cycle, it will definitely describe the dispersion phase. The intensity of PI with respect to SYTO-9 decreases at day 7 (3.8 ± 2.4505 a. u. PI, 6.2 ± 1.297 a. u. SYTO-9); thus, alive cells predominate dead cells at day 7. The last stage in the biofilm life cycle is the detachment phase, therefore, day 7 marks the beginning of a new cycle. Besides, biofilm thickness was assessed by z-stacks, and five different regions were evaluated with respect to each measured component in the biofilm (Fig. 4). The thickness according to SYTO-9 reached 6.05 ± 0.07638 μm in the first 3 days then decreased to ($5.4 \mu\text{m} \pm 0.18148$) at day 4, disproportional with the PI thickness as it increased from day 4 to 10.76 ± 0.85169 μm at day 6. These results were correlated with the intensities of both SYTO-9 and PI. Day 7 showed a rejuvenation for the biofilm by the increase in green color (alive cells) intensity and thickness (6.25 ± 1.297 a. u.; 11.185 ± 0.228 μm).

Consequently, a 2.5D structure of the biofilm revealed the same results, and $63\times$ images convey different layering

features in the same biofilm with time (Fig. 2). Day 1 and 2 showed dense cell connections, and day 3 showed black holes or channel like structures in the biofilm that increase with age (Fig. 5). $20\times$ and $60\times$ PI/SYTO-9 staining magnification images showed a decrease in mesh-like organization from day 4 to small clusters. Reformation of network structures was obvious on day 7. Using COMSTAT 2.1 software, the biomass ($\mu\text{m}^3/\mu\text{m}^2$) obtained showed an increase in dead cells at day 4 (23.15667 ± 6.075396 $\mu\text{m}^3/\mu\text{m}^2$) with a decrease in alive cells (22.75 ± 2.968956 $\mu\text{m}^3/\mu\text{m}^2$, day 3) (18.97 ± 5.713706 , 5.48 ± 3.098275 $\mu\text{m}^3/\mu\text{m}^2$, day 4 and 5, respectively). The dead-to-alive ratio begins to decrease by day 7 (5.22 ± 0.716961 $\mu\text{m}^3/\mu\text{m}^2$ dead, 11.95 ± 0.456691 $\mu\text{m}^3/\mu\text{m}^2$ alive) (Table 2).

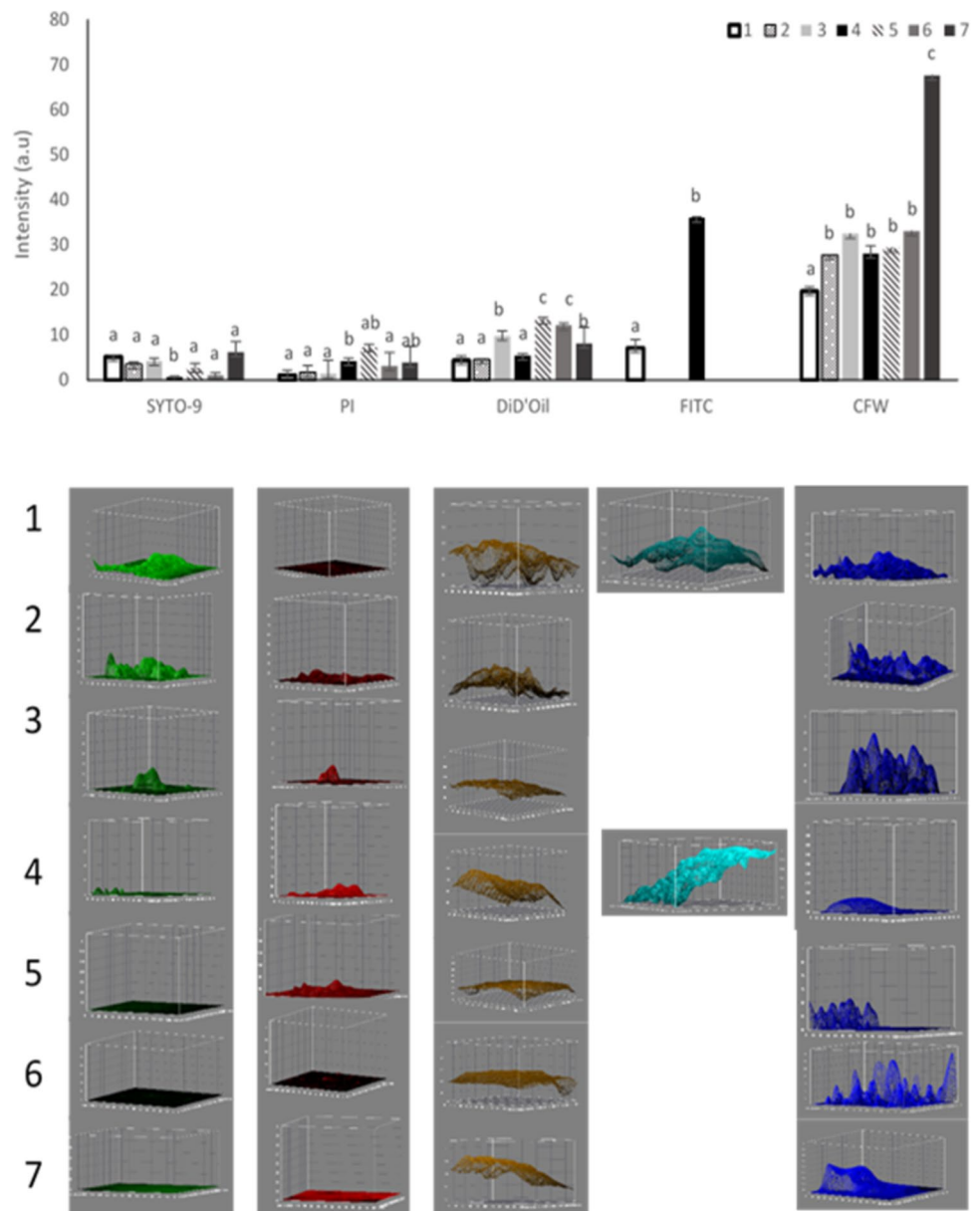
According to statistical analysis, PI showed a significant difference ($P < 0.05$) between the days in comparison to SYTO-9.

The staining with CFW targeting β -polysaccharide (blue fluorescent), which constitutes the slime component in *S. epidermidis* CIP 444 (Sadovskaya et al. 2006), revealed a non-significant fluctuation during the 3 days after culturing and a slight decrease following the detachment (28.1 a. u.). CFW intensity increased from day 6 (33.03 ± 2.162 a. u. to 67.6 ± 2.559 a. u.) at day 7, in which the re-establishment of the matrix took place as mentioned before. In addition, combining the 3 dyes together (cells plus polysaccharides) revealed a predominance for the polysaccharides with respect to cell count, during the studied period, as shown in the intensity percentages (supplementary file. 1). Regarding the lipid profile, DID'OIL fluorescence (orange) was low at the beginning (4.6 ± 0.2605 a. u. day 1; 4.8 ± 0.38 a. u. day 2), but it appeared intense during the biofilm detachment phase (13.43 ± 0.7995 a. u.) with a drop during the reconstruction period days 6 and 7 (12.02 ± 0.474 a. u., 8.13 ± 1.567 a. u., respectively). Finally, treating biofilm samples with FITC to estimate protein content at days 1 and 4 showed a dramatic increase in intensity at day 4 (35.9 ± 1.75 a. u.) compared with day 1 (7.1 ± 0.929 a. u.) (Fig. 4).

DID'OIL and FITC analyses showed a significant difference between the days ($P < 0.05$). When measuring the thickness with respect to DID'OIL intensity and FITC, we obtained similar results as the intensity measurement. On day 1, the biofilm thickness with respect to DID'OIL was 9.2 ± 0.06174 μm which increased in the detachment phase, reaching 15.2 ± 0.01681 μm at day 5, then decreased to 9.5 ± 0.15791 μm at day 7. The assessment of biofilm thickness after protein staining showed an increase from day 1 (6.8 ± 0.03199 μm) to day 4 (8.9 ± 0.03087 μm). However, it was not the case in CFW, which showed a gradual increase in intensity from day 4 with no significant change in thickness.

The average of the obtained intensities was added to constitute the biofilm composition for each day. Polysaccharides

Fig. 3 Intensity mean value for the fluorescence of the studied dyes corresponding to biofilm components of *S. epidermidis* CIP 444 presented in arbitrary units (a. u.). Area of observation field = 1.42 cm². Using the Duncan multiple range test, *P* value was calculated, *P* < 0.05 = significant difference. 3D structures of 63 × images for all days obtained from ImageJ software, an illustration revealing the distribution of biofilm components individually



form the major constituent among the studied components in a 24-h biofilm (52%), followed by proteins (18.9%). Lipids form a minor part of the mature biofilm (11.6%). For a 4-day-old biofilm, the protein content is the highest (48%), followed by polysaccharides (37.8%), and then lipids (7.27%). Concerning the relation between the dyes, the Pearson test showed a weak correlation between beta-polysaccharides and alive cells ($r=0.46$, 46%) and between dead cells and lipids ($r=0.43$, 43%), and no correlation with other components with time (Fig. 6). By calculating the roughness coefficient (R_a^*) the biofilm surface was assessed. *S. epidermidis* CIP 444 biofilm is not a uniform biofilm; the roughness coefficient increases with biofilm age until day 6, when it declines slightly (from 0.73 ± 0.31 to 0.59 ± 0.08),

thus a smoother surface at day 6. R_a^* re-increases at day 7 (Table 2).

A difference in the spatial distribution of biofilm components was spotted (Fig. 7A). These significant differences allow bacterial cell attitude to be featured in each stage. Each component occupies specific zones in the biofilm (Fig. 7). The major content, polysaccharide, forms a network that covers the biofilm on all its sides, where cells are imbedded in different layers, constructing mushroom-like structures. Whereas protein and lipid are distributed on the upper part of the slime network. The summary of intensities and 3D distribution of biofilm components is illustrated in Fig. 3. The merged channels (Fig. 7B) allow us to figure out how these components react with each other, and thus, showing

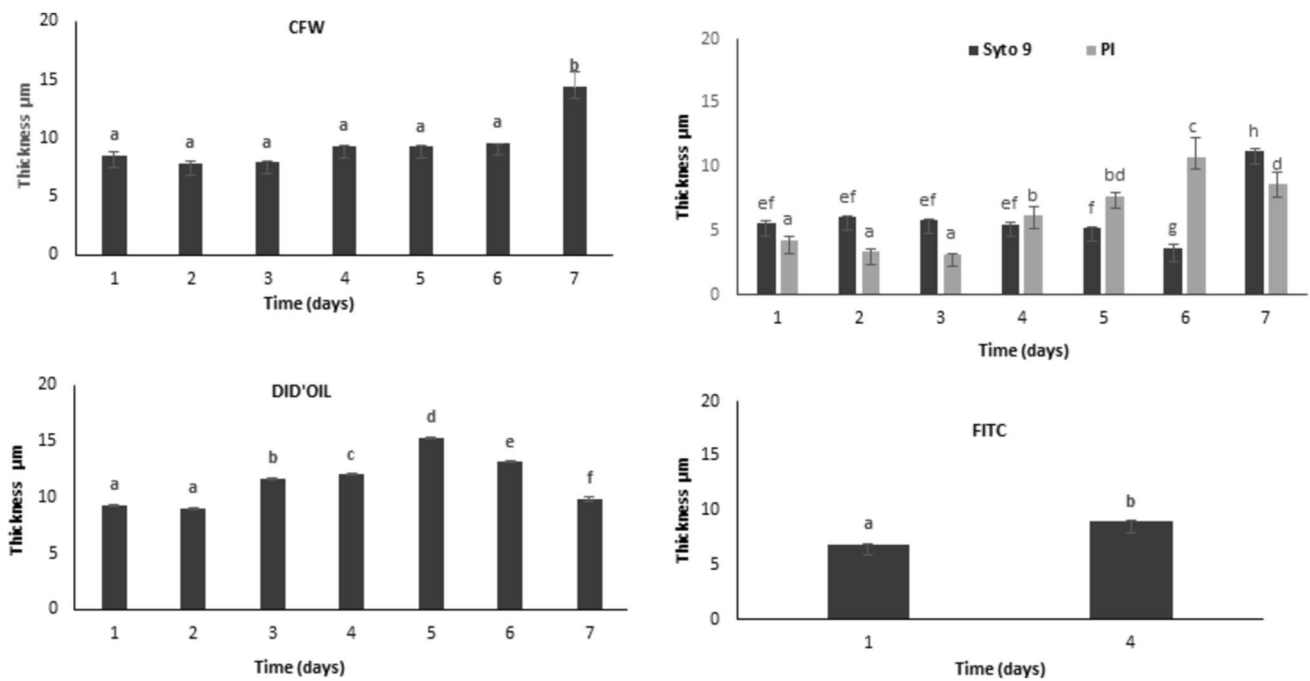
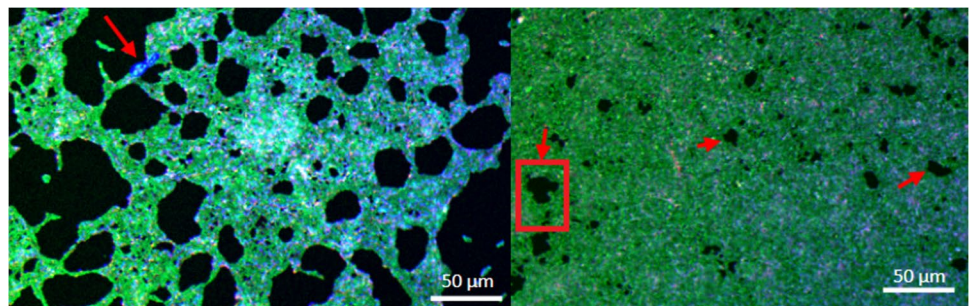


Fig. 4 Thickness of the biofilm with respect to all studied dyes, 40 z-stacks of horizontal plane images (512×512 pixels corresponding to $134.95 \mu\text{m} \times 134.95 \mu\text{m}$) with a z-step of $0.39 \mu\text{m}$ were acquired for each well from five different randomly chosen areas where the

maximum thickness (μm) of biofilm was determined directly from the confocal stack image. Three independent experiments with three replicates were performed for each sample during the biofilm life cycle on a 7-day period

Fig. 5 CLSM images ($20\times$) for *S. epidermidis* CIP 444 biofilm stained with Bac light bacterial viability kit and CFW. Red arrow (left) showing the polysaccharide link (blue), red arrow (right) showing pores (wide holes), and water channels (narrow holes) in the biofilm. Scale bar = $50 \mu\text{m}$



the importance of each component in each period of the study.

Biofilm establishment requires the production of components to construct the protective matrix, which is a combination of polysaccharides, nucleic acids, proteins, and lipids using a wide cascade of gene networks controlled by bacterial crosstalk through quorum sensing. Several matrix constituents are known to be potential virulence factors, and as a result, the matrix is crucial in the pathogenesis of both human and animal illnesses. The EPS-based matrix drives biofilm assembly. In order to provide an initial polymeric matrix that encourages microbial colonization and cell clustering, the EPS is initially generated on bacterial surfaces or released on the surface of attachment. While generating a core of EPS-embedded bacterial cells, continuous EPS synthesis progressively increases the matrix in three dimensions

and thus provides a supporting architecture to facilitate the growth of 3D clusters, aggregates, or microcolonies. Biofilms feature a distinctive 3D structure with towers that are sometimes compared to “mushrooms,” with fluid-filled pathways or channels between those towers (Otto 2009).

The biochemical composition of the biofilm plays a major role in its lifecycle, including antibiotic resistance and the release of virulence factors and toxins (Hobley et al. 2015). This paper focuses on the changes that occur when encountering *S. epidermidis* biofilm, which is now considered a main contributor to nosocomial infections, especially at the dispersion phase that forms a key to understanding biofilm virulence and thus controlling it. The results showed a variation in the cell count, along with the chemical composition of the biofilm at different stages. In a healthy biofilm, the number of alive cells is greater than the number of dead

Table 2 Biofilm parameters calculated from z-stack images using COMSTAT software

Days	Biomass $\mu\text{m}^3/\mu\text{m}^2$		Surface to biovolume ratio $\mu\text{m}^2/\mu\text{m}^3$		Roughness coefficient (R^{*2}) mean \pm SD							
	Mean \pm SD		Mean \pm SD		Mean \pm SD							
	Dead	Alive	Dead	Alive	Dead	Alive						
1	9.48	2.530771ac	13.25	2.632793ab	5.17102	5.841252a	1.028272ab	0.247917	\pm	1.096877	\pm	0.200365a
2	3.746667	0.981852bc	6.973333	0.821462bc	4.016667	0.554286a	0b	0.275667	\pm	2.27	\pm	0.20a
3	15.18	1.818433c	22.75	2.968956c	1.526667	0.309246a	0.270634a	0.288167	\pm	0.239	\pm	0.174712a
4	23.15667	6.075396d*	18.97333	5.713706bc	1.64	0.270555a	0.348473b	0.46	\pm	2.136667	\pm	0.08579ab
5	10.79667	1.8876bc	5.481667	3.098275b	2.03	0.230651a	1.19056c*	0.733333	\pm	3.856667	\pm	0.319729 cd
6	12.07667	2.462323bc	9.82	2.430062ab	1.773333	0.068069a	0.101489b	0.593333	\pm	2.21	\pm	0.087788bc
7	5.226667	0.716961a	11.95767	0.456691ab	4.313333	0.349619a	0.086603b	0.871667	\pm	2.2	\pm	0.064317d

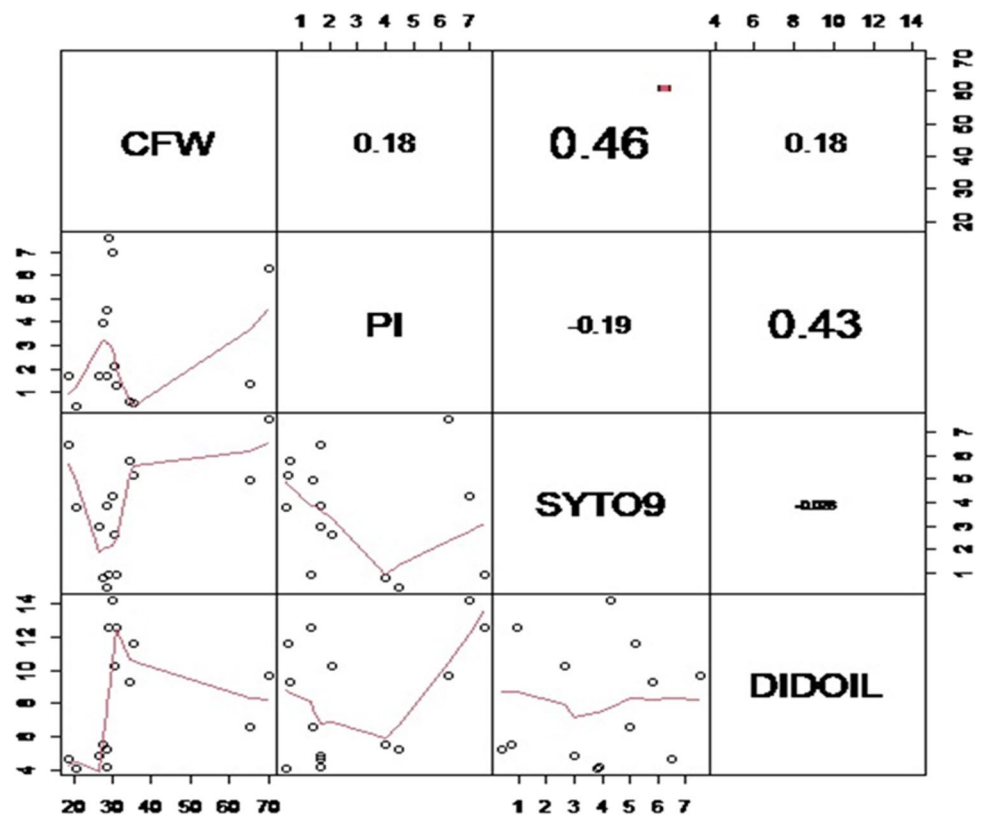
Letters correspond to statistical difference

Asterisk (*) corresponds to significant difference $p < 0.05$

cells during the first 3 days of incubation. The percentage of alive cells was dominant, but the count fluctuates slightly over time, indicating the bacterial cell cycle, as new cells emerge with the decay of others. It is well known that the metabolism and growth rate inside a biofilm are slow due to limited nutritional resources and as a protective strategy. The biofilm's complexity made it difficult to study. The green fluorescent (SYTO-9) indicates various bacterial modes, including those with active or slow metabolism, as well as those that are dormant and have no metabolic activity but are still alive. All of the studied features indicate that day 3 is the maturation stage at which the biofilm is saturated, which means it no longer has the capacity to grow, as a result of the quorum sensing system, which allows bacteria to sense cell density. Furthermore, when combining PI, SYTO-9, and CFW, 20 \times and 63 \times images revealed numerous black holes not covered with cells or slime. Some holes were narrow, forming a tunnel deep within the biofilm, while others were much wider (Fig. 5). Biofilms, as is well known, contain water-filled zones within and between bacterial clusters; these zones may be held together by EPS or co-adhesion between the bacteria in the aggregation (Foster and Kolenbrander 2004).

Channels or pores are often used terms to characterize water-filled biofilm architecture. Both channels and pores are essential for the survival of a biofilm since they provide water and nutrients for deeper cells in a dense biofilm. By definition, channels connect two locations and are typically narrow, whereas, pores are characterized by relatively large volumes that function as storage and emollient areas rather than connecting various locations. The black holes in the biofilm are mainly water channels appearing on days 1, 2, 3, and 7. It has been proposed that *P. aeruginosa* in biofilms lyses itself to form pores (Webb et al. 2003). Lately, the mechanism of pore development has been explained as a way to lessen the population of occupants in mature biofilms (Hobley et al. 2015), and this agrees with our results on day 3, and thus it is an indication of dispersion induction. With respect to the red fluorescent (PI), a slight increase in the dead cell count during the first 3 days of incubation is a normal fact with decreasing nutrient conditions, as mentioned so far. The rise in PI intensity, thickness, and biomass at days 4 and 5 with the decrease in SYTO-9 (alive cells) indicates dispersion and disintegration of the biofilm architecture, and this was confirmed by 63 \times images that showed the loss of aggregations and stacks of cells that were linked together to simpler clumps and even single cells. However, according to Rosenberg et al. PI staining sometimes binds extracellular DNA (eDNA), one of the components of bacterial extracellular polymeric substances (EPS), rather than being a reliable indicator of membrane integrity (Rosenberg et al. 2019). In fact, early bacterial adhesion, microcolony formation, and aggregation, as well as shaping the general

Fig. 6 Pearson's correlation test describing the relation between the used dyes. $r=0.9^*$, close pattern of distribution means strong correlation



biofilm architecture, are all crucial phases in the production of biofilms (Qin et al. 2007; Das et al. 2010; Whitchurch et al. 2002). According to the studies, the release of eDNA encourages early bacterial attachment and aggregation by altering electrostatic and hydrophobic interactions between the bacterium and the surface (Das et al. 2010; Liu et al. 2008). These justifications agree with our findings, as PI intensity increases from day 4 (4.23 a. u.) which represents a combination of dead and eDNA (released from dead cells). The increase in β -polysaccharides at day 6 (33.06 a. u.), as well, is a sign of new establishment after the disintegration and dispersion of the biofilm. Nevertheless, bacterial adaptation to harsh, stressful conditions is achieved by incorporating free fatty acids from the environment to its membrane, in order to decrease membrane fluidity and reserve its energy for enhancing bacterial survival and resistance (Brinster et al. 2010; Dubois-Brissonnet et al. 2016). Lipids constitute a minor proportion in the staphylococcal biofilm; our results demonstrate an increase in the lipid profile from day 4 reaching a maximum at day 5 (13.43 a. u.), where we assumed dispersion is taking place. As mentioned by Alim et al. (2018), lipid promotes cell–cell signaling during *Candida albican* biofilm formation and increases hydrophobicity by changing the lipid composition of the cells to facilitate re-attachment to the surface, adaptation to stressful conditions, and maintain survival (Boles et al. 2004). The rise in protein content

for a 4-day-old biofilm (35.9 ± 1.75 a. u.) with respect to a 1-day-old biofilm (7.1 ± 0.929 a. u.) has two aspects. First, behind biofilm dispersion is the expression of diverse proteins that promote matrix disintegration, such as enzymes (proteases, nucleases), specific ligands, transporters, and other factors involved in quorum sensing to achieve this target. On the other side, a strategy used by several bacterial species to give the biofilm structural integrity/rigidity is the production of protein fibers that serve as a scaffold for the attachment of cells and other matrix elements (Barnhart and Chapman 2006; Branda et al. 2006; Borlee et al. 2010). Therefore, as we proved, the reformation of a new biofilm requires the incorporation of new proteins, and thus a wide variety of proteins responsible for dispersion and formation are present at this stage. The analysis of the results assumes that this protein profile will continue to increase after day 4, until a new biofilm is formed (this assumption needs to be validated by experimental work for the other days). Based on the intensities of the 5 dyes, the composition variation in the biofilm components with time was determined. The major constituent of *S. epidermidis* CIP 444 biofilm on day 1 is the beta- polysaccharides (β -1,6-linked N-acetylglucosamine residues), as mentioned by Sadovskaya et al. in which *S. epidermidis* CIP 444 produces large quantities of PIA (Sadovskaya et al. 2006), and this in fact promotes the accumulation and virulence of the biofilm. Polysaccharides in the biofilm, or “slime,” are the protective barrier

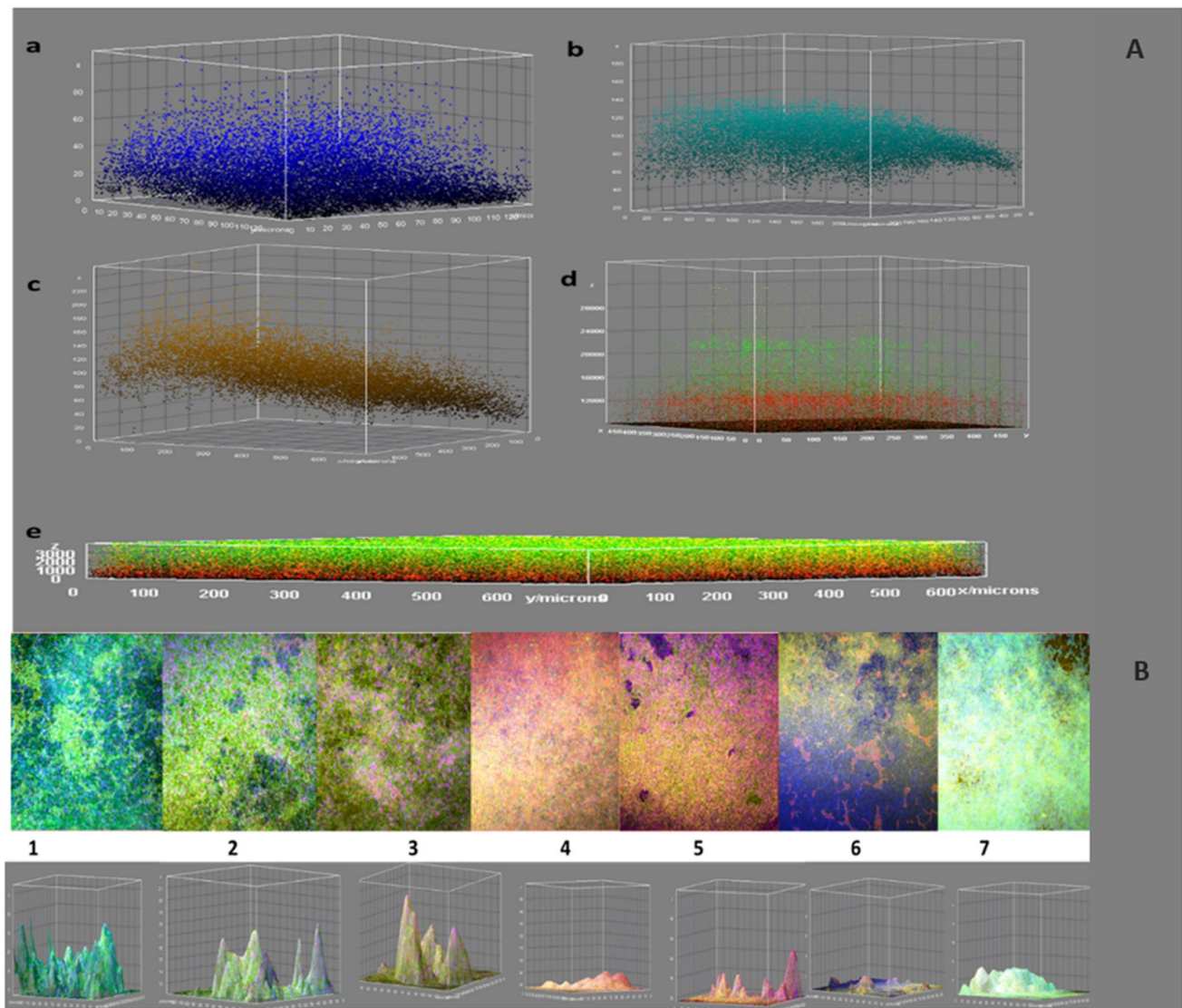


Fig. 7 Distribution of *S. epidermidis* CIP 444 biofilm components according to 63 \times confocal images after fluorescent staining using ImageJ software. (a) polysaccharide, (b) protein, (c) lipids, (d) dead (red), and viable cells (green), (e) vertical cross section of the biofilm showing dead and viable cells (A). CLSM 63 \times images of *S. epi-*

dermidis CIP 444 biofilm showing the cells with the matrix, merging channels of used dyes with the interactive 3D surface plot. Ch1: PI (red), Ch2: SYTO9 (green), Ch3: CFW (blue), Ch4: DID'OIL (yellow) (B)

that engulfs the cells to maintain survival. Consequently, as shown on day 1, it forms the major component. Although day 4 showed a slight decrease in the polysaccharide (28 a. u.) in comparison with the protein profile (35.9 a. u.), that is mainly due to the decrease in viable cells and the surrounding network in the biofilm promoting dispersion. In general, during detachment, the matrix will be degraded by a wide variety of enzymes and the protective layer will break down, so cells will be free from the assembly. The second major component is the protein content on day 1. Yet, the protein profile for the whole experiment was not examined, but the increase in its quantity at day 4 assures

that it plays an important role in biofilm dispersion and scaffolding. Cells, eDNA, and lipids form the lower portion of the whole biofilm. Even though it forms a low percent of the biofilm lipids in *S. epidermidis*, it is of great importance. Lipoteichoic acid (LTA), for example, is a main contributor to the immunomodulatory response of *S. epidermidis*. Gram-positive bacteria's LTA plays a large and crucial role in maintaining cellular homeostasis. LTA controls the net charge of the cell wall to prevent cationic antimicrobial peptides from attacking the cytoplasmic membrane, regulates cellular division, and protects against heat and osmotic stress. In our study, the thickness of the biofilm was not

correlated with the fluorescent intensities in all cases (CFW had no significant changes in thickness), and this was illustrated by Krasowski et al. (Krasowski et al. 2021) where various regions in the same biofilm are occupied by various cellular densities, and staphylococcal biofilm is in most cases heterogeneous with a hill-like landscape. Accordingly, we examined the topographical surface of the biofilm, stained for cells and slime, for the same study period by using ZEN 3.4 blue edition, and the results showed differences in the spatial distribution of the biofilm as a function of time. Moreover, the roughness coefficient was calculated by COMSTAT to reveal surface irregularities. Supplementary file 2 shows a clear illustration for the morphology of *S. epidermidis* CIP 444 biofilm; it describes the spatial distribution of the cells and slime as one unit (mixed channels, Supplementary file 2a–g) or distinct (each component alone, Supplementary file 2 h) showing dead cells, alive cells, and the slime. Roughness (that measures biofilm hills and valleys) increased as biofilm aged, showing a more heterogeneous appearance (Table 2). Chemical features related to EPS within a 3D matrix framework, create unified yet incredibly varied landscapes.

The cause behind these surface occupations is bacterial amyloids. Bacterial amyloids help in the biofilm's life cycle; they can mediate toxicity and cell-to-cell contacts within the biofilm and are the main structural elements of the biofilm matrix. Additionally, amyloids are in charge of the biofilm's spatial organization, morphological differentiation, surface characteristics, and virus defense (Biesecker et al. 2018; Deshmukh et al. 2018). This can explain changes and alterations in the biofilm morphology. One of the important amyloids in *S. epidermidis* is the accumulation associated protein, which has a role in scaffolding and the construction of aerial structures inside the biofilm (Maury 2009). Moreover, to create nutritional and chemical gradients, including oxygen, pH, signaling molecules, inorganic ions, metabolites, and other solutes, throughout the biofilm's 3D architecture, EPS can sequester or trap various substances while also regulating the flow of various molecules inside the biofilm. The biofilm matrix's capacity as a local nutrition store for different biomolecules, such as fermentable polysaccharides, is another important chemical function (Rumbaugh and Sauer 2020). This can explain the cell distribution in the biofilm as shown in (Fig. 7A), dead cells occupy the lower parts of the biofilm in a vertical cross-section, while viable cells account for more exposed regions. Deep in the biofilm, the availability of oxygen and nutrients decreases even though channels serve as an active passage to nourish embedded stacks; therefore, the lysed cells will contribute to matrix modeling and as a nutrient source for other cells during unfavorable conditions. Furthermore, dormant cells inhabited the lower parts of dense viable stacks, since it requires less energy and oxygen to maintain survival, yet,

the complexity of biofilm arises from the different bacterial stages that communicate in stressful conditions in a poorly understood way.

A 3D surface plot of different day samples showed the distribution of lipids, proteins, and polysaccharides throughout the biofilm. As shown in Fig. 3, lipids and proteins are not attached to the surface, whereas the distribution of polysaccharides is all over the biofilm. This result describes the main backbone (polysaccharide) that links the cells together and promotes the production of other EPS components. Hence, lipids and proteins will be intercalating the slime mesh. Figure 7B shows an illustration of the matrix component organization in the biofilm. The latter is coordinated by quorum sensing as we mentioned so far, this complex system in the bacteria allow it to sense changes in cell density and thus promote changes in biofilm matrix components and organization according to the suitable state. So, it forms another key to exploring the dispersion state of the biofilm and controlling its virulence. Finally, quorum sensing, which regulates cell–cell communication in bacterial biofilms, is still under investigation; however, dispersion is still an obstacle that is not well understood.

Conclusion

This study investigated the biofilm dispersion time in the clinical strain *Staphylococcus epidermidis* CIP 444, in addition to changes in the biofilm structure and composition over a period of 7 days. Days 4 and 5 of the biofilm ages impose remarkable changes in cell number and matrix composition. These results ensure a repetitive mode in the biofilm cycle under stress conditions, which increases the possibility of recurrent infections at the same body site. Therefore, additional research should concentrate on the dynamics of matrix control, structural organization, and remodeling using recent technical developments, including imaging, spectroscopy-based techniques, and computer analysis. Yet, overall, biofilm is a complex architecture that needs more studies, especially at the dispersion stage, to explore new bacterial strategies that will assist in finding a solution for these resistant communities.

Supplementary Information The online version contains supplementary material available at <https://doi.org/10.1007/s10123-023-00433-2>.

Acknowledgements We are grateful for the support of. Dr. Jean Benoît Peltier, UMR IPSiM, Université de Montpellier, Institut Agro, CNRS, INRAE, 2 Place Pierre Viala, 19 CEDEX 2, 34060 Montpellier, France.

Authors' contributions S.J performed the experimental work, wrote the main manuscript and prepared all figures under the supervision of A.C, M.K and A.K. F.A was responsible for the statistical analysis, K.Z, M.S and V.D contribute in confocal microscopy.

Data availability Data is available upon request.

Declarations

Ethics approval and consent to participate There are no human or animal experimental work in this study.

Consent for publication The publisher has the permission of the author to publish the work.

Competing interests The authors declare that there are no conflicts of interest.

References

- Alim D, Sircaik S, Panwar SL (2018) The significance of lipids to biofilm formation in *Candida albicans*: an emerging perspective. *J of Fungi* 4(4):140
- Azeredo J, Azevedo NF, Briandet R, Cerca N, Coenye T, Costa AR, Sternberg C (2017) Critical review on biofilm methods. *Crit Rev Microbiol* 43(3):313–351
- Barnhart MM, Chapman MR (2006) Curli biogenesis and function. *Annu Rev Microbiol* 60:131–147
- Ben-Sahil A, Mohamed A, Beyenal H (2020) Three-dimensional biofilm image reconstruction for assessing structural parameters. *Biotechnol Bioeng* 117(8):2460–2468
- Biesecker SG, Nicastro LK, Wilson RP, Tükel Ç (2018) The functional amyloid curli protects *Escherichia coli* against complement-mediated bactericidal activity. *Biomolecules* 8(1):5
- Boles BR, Thoendel M, Singh PK (2004) Self-generated diversity produces “insurance effects” in biofilm communities. *Proc Natl Acad Sci* 101(47):16630–16635
- Borlee BR, Goldman AD, Murakami K, Samudrala R, Wozniak DJ, Parsek MR (2010) *Pseudomonas aeruginosa* uses a cyclic-di-GMP-regulated adhesin to reinforce the biofilm extracellular matrix. *Mol Microbiol* 75(4):827–842
- Branda SS, Chu F, Kearns DB, Losick R, Kolter R (2006) A major protein component of the *Bacillus subtilis* biofilm matrix. *Mol Microbiol* 59(4):1229–1238
- Brinster S, Lamberet G, Staels B, Trieu-Cuot P, Gruss A, Poyart C, Brinster et al. (2010) Reply. *Nature*, 463(7279), E4–E4
- Byers JD, Ratner BD (2004) Bioinspired implant materials befuddle bacteria. 230 *ASM News*
- Castelli P, Caronno R, Ferrarese S, Mantovani V, Piffaretti G, Tozzi M, Sala A (2006) New trends in prosthesis infection in cardiovascular surgery. *Surgical Infections* 7(Supplement 2):S-45
- Das T, Sharma PK, Busscher HJ, Van Der Mei HC, Krom BP (2010) Role of extracellular DNA in initial bacterial adhesion and surface aggregation. *Appl Environ Microbiol* 76(10):3405–3408
- Deshmukh M, Evans ML, Chapman MR (2018) Amyloid by design: intrinsic regulation of microbial amyloid assembly. *J Mol Biol* 430(20):3631–3641
- Dhekane R, Mhade S, Kaushik KS (2022) Adding a new dimension: multi-level structure and organization of mixed-species *Pseudomonas aeruginosa* and *Staphylococcus aureus* biofilms in a 4-D wound microenvironment. *Biofilm* 4:100087
- Dubois-Brissonnet F, Trotier E, Briandet R (2016) The biofilm lifestyle involves an increase in bacterial membrane saturated fatty acids. *Front Microbiol* 7:1673
- Ecker DJ, Carroll KC (2005) Investments in high-payoff technologies could reduce toll of infections. *ASM News* 71(12):576–581
- Foster JS, Kolenbrander PE (2004) Development of a multispecies oral bacterial community in a saliva-conditioned flow cell. *Appl Environ Microbiol* 70(7):4340–4348
- Gonzalez-Machado C, Capita R, Riesco-Pelaez F, Alonso-Calleja C (2018) Visualization and quantification of the cellular and extracellular components of *Salmonella Agona* biofilms at different stages of development. *PLoS ONE* 13(7):e0200011
- Heydorn A, Nielsen AT, Hentzer M, Sternberg C, Givskov M, Ersbøll BK, Molin S (2000) Quantification of biofilm structures by the novel computer program COMSTAT. *Microbiology* 146(10):2395–2407
- Hobley L, Harkins C, MacPhee CE, Stanley-Wall NR (2015) Giving structure to the biofilm matrix: an overview of individual strategies and emerging common themes. *FEMS Microbiol Rev* 39(5):649–669
- Jeckel H, Drescher K (2021) Advances and opportunities in image analysis of bacterial cells and communities. *FEMS Microbiol Rev* 45(4):fuaa062
- Krasowski G, Migdał P, Woroszyło M, Fijałkowski K, Chodaczek G, Czajkowska J, ... Junka A (2021). The processing of staphylococcal biofilm images from fluorescence and confocal microscopy to assess in vitro efficacy of antiseptic molecules. *Biorxiv*, 2021–1
- Liu Y, Harnisch F, Fricke K, Sietmann R, Schröder U (2008) Improvement of the anodic bioelectrocatalytic activity of mixed culture biofilms by a simple consecutive electrochemical selection procedure. *Biosens Bioelectron* 24(4):1006–1011
- Mack A, Choffnes ER, Hamburg MA, Relman DA (eds) (2009) Microbial evolution and co-adaptation: a tribute to the life and scientific legacies of Joshua Lederberg: workshop summary. National Academies Press
- Maury CPJ (2009) The emerging concept of functional amyloid. *J Intern Med* 265(3):329–334
- Mountcastle SE, Vyas N, Villapun VM, Cox SC, Jabbari S, Sammons RL, Kuehne SA (2021) Biofilm viability checker: an open-source tool for automated biofilm viability analysis from confocal microscopy images. *Npj Biofilms and Microbiomes* 7(1):44
- Nicolle LE (2012) Urinary catheter-associated infections. *Infect Dis Clin* 26(1):13–27
- O’Toole G, Kaplan HB, Kolter R (2000) Biofilm formation as microbial development. *Annu Rev Microbiol* 54(1):49–79
- Otto M (2009) *Staphylococcus epidermidis*—the accidental pathogen. *Nat Rev Microbiol* 7(8):555–567
- Qin Z, Yang X, Yang L, Jiang J, Ou Y, Molin S, Qu D (2007) Formation and properties of in vitro biofilms of ica-negative *Staphylococcus epidermidis* clinical isolates. *J Med Microbiol* 56(1):83–93
- R Core Team (2021). R: a language and environment for statistical computing. R Foundation for statistical Computing, Vienne, Austria. URL <https://www.R-project.org/>
- Rogers KL, Fey PD, Rupp ME (2009) Coagulase-negative staphylococcal infections. *Infect Dis Clin North Am* 23(1):73–98
- Rogers GB, Hoffman LR, Whiteley M, Daniels TW, Carroll MP, Bruce KD (2010) Revealing the dynamics of polymicrobial infections: implications for antibiotic therapy. *Trends Microbiol* 18(8):357–364
- Rohde H, Frankenberger S, Zähringer U, Mack D (2010) Structure, function and contribution of polysaccharide intercellular adhesin (PIA) to *Staphylococcus epidermidis* biofilm formation and pathogenesis of biomaterial-associated infections. *Eur J Cell Biol* 89(1):103–111
- Rojas M, Del Valle D (2009) Betalactamasas tipo AmpC: generalidades y métodos para detección fenotípica. *Rev Soc Venez Microbiol* 29(2):78–83
- Rosenberg M, Azevedo NF, Ivask A (2019) Propidium iodide staining underestimates viability of adherent bacterial cells. *Sci Rep* 9(1):1–12

- Rumbaugh KP, Sauer K (2020) Biofilm dispersion. *Nat Rev Microbiol* 18(10):571–586. <https://doi.org/10.1038/s41579-020-0385-0>
- Rupp ME, Archer GL (1994) Coagulase-negative staphylococci: pathogens associated with medical progress. *Clin Infect Dis* 19:231–243
- Sadovskaya I, Chaignon P, Kogan G, Chokr A, Vinogradov E, Jabbouri S (2006) Carbohydrate-containing components of biofilms produced in vitro by some staphylococcal strains related to orthopaedic prosthesis infections. *FEMS Immunol Med Microbiol* 47(1):75–82
- Sadovskaya I, Faure S, Watier D, Leterme D, Chokr A, Girard J, Jabbouri S (2007) Potential use of poly-N-acetyl- β -(1, 6)-glucosamine as an antigen for diagnosis of staphylococcal orthopedic-prosthesis-related infections. *Clin Vaccine Immunol* 14(12):1609–1615
- Safdar N, Maki DG (2002) Inflammation at the insertion site is not predictive of catheter-related bloodstream infection with short-term, non-cuffed central venous catheters. *Crit Care Med* 30(12):2632–2635
- Suryabrata S (2008) Metodologi penelitian
- Vorregaard M (2008) Comstat2-a modern 3D image analysis environment for biofilms: Technical University of Denmark, DTU, DK-2800 Kgs. Lyngby, Denmark. <http://www.comstat.dk/>
- Webb JS, Thompson LS, James S, Charlton T, Tolker-Nielsen T, Koch B, Kjelleberg S (2003) Cell death in *Pseudomonas aeruginosa* biofilm development. *J Bacteriology* 185(15):4585–4592
- Wenzel RP (2007) Health care-associated infections: major issues in the early years of the 21st century. *Clin Infect Dis* 45(Supplement_1):S85–S88
- Whitchurch CB, Tolker-Nielsen T, Ragas PC, Mattick JS (2002) Extracellular DNA required for bacterial biofilm formation. *Science* 295(5559):1487–1487
- World Health Organization 2022, Mar https://apps.who.int/gb/MSPI/pdf_files/2022/03/Item1_07-03.pdf
- Zhang X, Bishop PL, Kupferle MJ (1998) Measurement of polysaccharides and proteins in biofilm extracellular polymers. *Water Sci Technol* 37(4–5):345–348

Publisher's Note Springer Nature remains neutral with regard to jurisdictional claims in published maps and institutional affiliations.

Springer Nature or its licensor (e.g. a society or other partner) holds exclusive rights to this article under a publishing agreement with the author(s) or other rightsholder(s); author self-archiving of the accepted manuscript version of this article is solely governed by the terms of such publishing agreement and applicable law.